

# Ferroelectricity of polycrystalline $\text{GdMnO}_3$ and multifold magnetoelectric responses

L. Lin · L. Li · Z.B. Yan · Y.M. Tao · S. Dong · J.-M. Liu

Received: 20 May 2012 / Accepted: 16 November 2012 / Published online: 28 November 2012  
© Springer-Verlag Berlin Heidelberg 2012

**Abstract** The multiferroic behaviors of polycrystalline  $\text{GdMnO}_3$  are investigated by focusing on the ferroelectric response to the spin ordering sequence and external magnetic field. The polarization current shows sensitive response to both the Mn cycloidal spin order and Gd antiferromagnetic (AFM) order. The complicated magnetoelectric behaviors suggest that the Mn cycloidal spin order can be modulated by the Gd AFM order at low temperature via the Gd–Mn spin interaction. Due to the possible disorder and defects in polycrystalline nature, polycrystalline  $\text{GdMnO}_3$  may accommodate the cycloidal spin order in addition to the A-type AFM order at Mn sites, as illustrated by simulation based on the two-orbit double exchange model and measured hysteresis loops of polarization against magnetic field, indicating the switching of the ferroelectric domains coupled with the magnetic domains in response to magnetic field.

## 1 Introduction

Type II multiferroics, in which magnetic and ferroelectric (FE) orders couple intrinsically, have been retrieving spe-

cific attentions recent years not only for promising technological potentials but more from fundamental research interests [1–4]. The major advantage of type II multiferroics is the interactive control of FE polarization ( $P$ ) (magnetization  $M$ ) by magnetic field  $H$  (electric field  $E$ ). Since the discovery of such an effect in  $\text{TbMnO}_3$  [5], a number of complex transition metal oxide multiferroics have been synthesized and the major physics underlying these materials is being unveiled [6–12]. One of the common features in these multiferroics is that  $P$  arises from specific spin orders via spin-correlated mechanisms, in particular in noncollinear cycloidal spin (CS) order via the inverse Dzyaloshinskii–Mariya interaction mechanism (*asymmetrical exchange striction*) [13, 14] or E-type antiferromagnetic (E-AFM) order via the *symmetric exchange striction* [15, 16].

The representative multiferroics to illustrate above phenomena go to orthorhombic perovskite rare-earth manganites  $\text{RMnO}_3$  ( $Pbnm$  symmetry). Upon decreasing  $R$ -site ionic size ( $R_A$ ), the Mn spin order evolves from A-type antiferromagnetic (A-AFM) order ( $R = \text{La to Gd}$ ) to CS order ( $R = \text{Tb and Dy}$ ) and eventually toward E-AFM order ( $R = \text{Ho and smaller}$ ), due to the competing spin interactions associated with distorted  $\text{GdFeO}_3$ -type lattice including the Jahn–Teller active distortion [17]. For the CS order and E-AFM order, large  $P$  and gigantic magnetoelectric (ME) effect were repeatedly identified. In spite of this simple scenario, however, realistic situation is more complicated. Two issues are worthy of addressing. First, the ground state of  $\text{RMnO}_3$  is essentially determined by multifold spin interactions which are relevant with  $R_A$  in a well-defined way, and thus the ground state is on the edge of degenerate states. For instance, in the phase diagram,  $\text{GdMnO}_3$  (GMO) is designated to the A-AFM order but close to the boundary between the A-AFM order and CS order [4, 18]. Due to

---

L. Lin · L. Li · Z.B. Yan · Y.M. Tao · J.-M. Liu (✉)  
Laboratory of Solid State Microstructures, Nanjing University,  
Nanjing 210093, China  
e-mail: liujm@nju.edu.cn

L. Li · J.-M. Liu  
Institute for Advanced Materials, South China Normal University,  
Guangzhou 510006, China

S. Dong  
Department of Physics, Southeast University, Nanjing 211189,  
China

inevitable chemical disorder and defects, the two orders are easily inter-transited. Recent experiment on  $\text{Nd}_{1-x}\text{Y}_x\text{MnO}_3$  did evidence the coexistence of the A-AFM phase and CS phase, given the fact that the averaged ionic size of  $R$ -site ( $\text{Nd}_{1-x}\text{Y}_x$ )<sup>3+</sup> at  $x = 0.5$  is identical to  $\text{Gd}^{3+}$  in  $\text{GdMnO}_3$  [19]. In fact, various groups confirmed that GMO does have nonzero  $P$  at low temperature ( $T$ ) although the data are scattering and interpretation is authors-dependent [20–23]. However, no clear interpretation for this ferroelectricity is available.

Second, the magnetic ground state and multiferroic behaviors depend also on the  $4f$ -spins of rare-earth. Experiments on  $\text{DyMnO}_3$  and  $\text{HoMnO}_3$  revealed that the polarization comes not only from the CS order at  $\text{Mn}^{3+}$  site but more from the  $\text{Mn}^{3+}$ – $R^{3+}$  spin interaction [24–27]. Due to this  $\text{Mn}^{3+}$ – $R^{3+}$  spin interaction, the  $R^{3+}$  spin ordering if any would impose modulation of the  $\text{Mn}^{3+}$  spin order, thus leading to additional ME effect associated with the  $R^{3+}$  spin ordering. This fact is beyond conventional understanding which is irrelevant of  $R^{3+}$   $4f$ -spins, and thus raises challenges to conventional microscopic mechanism for ferroelectricity. It is noted that  $\text{Gd}^{3+}$ ,  $\text{Dy}^{3+}$ , and  $\text{Ho}^{3+}$ , etc. all have big moments and the  $R^{3+}$ – $\text{Mn}^{3+}$  spin interaction may play substantial roles in some cases, but such roles have been less concerned in terms of multiferroic generation [28–31].

Keeping in mind these two issues, GMO can be a good candidate for revealing the underlying physics. From the magnetic phase diagram of  $\text{RMnO}_3$ , GMO locates in the immediate vicinity of the phase boundary between the A-AFM order and long-wavelength CS order, and its ground state should be the A-AFM ordered phase [4, 18]. The reason why GMO exhibits multiferroicity at low  $T$  remains not yet well understood. On the other hand, several recent works on the multiferroicity of GMO were reported. So far, earlier studies on GMO mainly addressed single crystal samples and confusing multiferroic anomalies were observed. For example, it was observed [20] that nonzero polarization current (polarization  $P$ ) appears only within  $5.1 \text{ K} < T < 8.2 \text{ K}$  if the poling field onto the sample is maintained down to the lowest temperature ( $T$ , e.g.,  $\sim 2 \text{ K}$ ) in experiments. However, if the poling is imposed only down to  $T \sim 7 \text{ K}$ , nonzero current can persist up to  $T \sim 23 \text{ K}$ . Differently, another investigation [23] revealed nonzero current over the whole  $T$ -range below  $T \sim 14 \text{ K}$ . These results suggest that the  $\text{Gd}^{3+}$  AFM ordering should occur at  $T_{\text{Gd}} \sim 7 \text{ K}$ , and this ordering sequence obviously affects the Mn CS order, thus the ferroelectricity. Although no good consistency between the data from various groups is obtained, it seems that the CS order of the Mn spins depends on the  $\text{Gd}^{3+}$  AFM order, indicating clearly the substantial role of the  $\text{Mn}^{3+}$ – $\text{Gd}^{3+}$  spin interaction in modulating the Mn CS order. It should be noted that the  $4f$ -spin order is usually fragile against external magnetic field which can easily melt the  $\text{Gd}^{3+}$  AFM order at  $T < T_{\text{Gd}}$ .

Furthermore, a big challenge to probe the magnetic structure of GMO is from the strong scattering from the  $\text{Gd}^{3+}$  spins. Even so, recent X-ray resonant magnetic scattering investigations [21, 32] did disclose the role of the Gd spin ordering in enhancing the ferroelectricity at low  $T$ , and in particular in driving the Mn CS order with wave-vector  $\tau_{\text{Mn}} = 1/4$  along the  $b$ -axis [21]. This also confirmed the dependence of the Mn CS order on the Gd spin order.

In this work, we will revisit the multiferroicity of polycrystalline GMO to discuss the above two issues. First, we revisit the problem of ferroelectricity in GMO and deal with its  $T$ - and  $H$ -dependent behaviors. We will discuss the observed phenomena by consulting to the complicated magnetoelectric responses in GMO. Considering the fact that GMO favors the A-AFM order but close to the boundary between the A-AFM order and CS order [4, 18], we choose polycrystalline GMO rather than single crystal one as the object of the present work. We argue that polycrystalline GMO may accommodate the coexisting A-AFM order and CS order and such a coexistence can be sensitive to disorder and defects in the samples. The polycrystalline samples have higher density of such disorder and defects than the single crystals, allowing more significant phase coexisting behaviors. Based on our sufficient data on the ferroelectricity in response to both the Gd spin order and Mn spin order as well as external magnetic field, we will utilize the semiquantum two-orbit double exchange model to simulate such a disorder/defects induced phase existence. We will also present relevant data on the ME effect to support the simulated results.

On the other hand, a choice of polycrystalline samples would also bring some extrinsic effects into the experimental phenomena. For instance, the grain boundaries may pin mechanically the FE domains and impose extrinsic artifacts to the measured data. These artifacts may be the origins for the observed ME phenomena such as the multiferroic hysteresis behaviors to be addressed below, thus bringing some questions on the measured data. However, clarifying all these questions seems to be challenging and tedious. In order to clarify this issue, as an alternative approach, we perform parallel measurements on polycrystalline  $\text{Gd}_{0.95}\text{Tm}_{0.05}\text{MnO}_3$  (GTMO) samples synthesized under the conditions identical to GMO in the present experiments. The microstructures of the polycrystalline GMO and GTMO samples are almost identical. Details of the relevant experiments on the multiferroic phase transitions and possible phase-coexistence in GTMO were reported in our recent work [33]. The GTMO at 5 % Tm doping level was demonstrated to be dominated with the  $ab$ -plane CS order coexisting with minor A-AFM phase. In this case, it is expected that the GTMO sample may also show the multiferroic hysteresis. This fact will partially exclude the possibility that the evidences supporting our claim on the coexisting A-AFM order and CS order in

polycrystalline GMO are solely due to the some artifacts associated with, e.g., grain boundaries of the samples.

## 2 Experimental details

We focus on polycrystalline GMO samples which were synthesized by conventional solid state reaction. The GMTO samples used for comparison study were synthesized under the identical conditions. In details, stoichiometric amount of Gd<sub>2</sub>O<sub>3</sub> and Mn<sub>3</sub>O<sub>4</sub> were mixed, grounded, and presintered twice at 1000 °C and 1250 °C for 24 h, then pressed into pellets and calcined at 1300 °C for additional 24 h or longer. The sample show high quality with density higher than ~95 % of the theoretical one. The crystal structure was checked using X-ray diffraction (XRD) (Bruker Corporation) equipped with Cu  $K_{\alpha}$  radiation at room temperature and the high quality crystallinity and  $Pbnm$  symmetry are obtained. The grain size was measured using field-emission scanning electron microscopy, and we prepared several samples of different grain sizes from 100–600 nm, and all the samples have almost the same electrical and magnetic behaviors. This feature is critical in order to exclude if any the grain boundary effect on the property fluctuations from sample to sample.

The magnetic measurement including the  $M$ – $H$  and  $M$ – $T$  dependences was performed with the superconducting quantum interference device magnetometer (SQUID, Quantum Design Inc.). The specific heat  $C$  as a function of  $T$  was evaluated using the physical properties measurement system (PPMS, Quantum Design Inc.). The dielectric constant ( $\epsilon$ ) was probed using HP4294A impedance analyzer attached to the PPMS, while polarization  $P$  was evaluated utilizing the pyroelectric current method detected by Keithley 6514 electrometer attached to the PPMS, also. For this measurement, the  $T$ - and  $H$ -dependences of  $P$  were obtained by integrating the pyroelectric current through warming the samples at rates of 2–6 K/min (magnetic field scanning rate of 100 Oe/s) after a cooling sequence under a poling field  $E \sim 10$  kV/cm from high temperature. In our measurements, sputtered gold electrodes on the both sides of the disk-like samples were used.

## 3 Results and discussion

We first look at the magnetic and ferroelectric properties. The measured specific heat ( $C$ ) and  $M$  data under the zero-field cooled (ZFC) and field cooling (FC) conditions, as a function of  $T$ , are plotted in Fig. 1(a). For the ZFC case,  $M$  gradually increases with decreasing  $T$  and exhibits a broad peak at  $T \sim 7$  K. The ZFC and FC  $M$ – $T$  curves begin to split at  $T \sim 23$  K. It is known that Gd<sup>3+</sup> ion has much bigger magnetic moment ( $7.94\mu_B$ ) than Mn<sup>3+</sup> ion ( $\sim 2.0\mu_B$ ), and thus the measured  $M$  signals come mainly from Gd<sup>3+</sup>

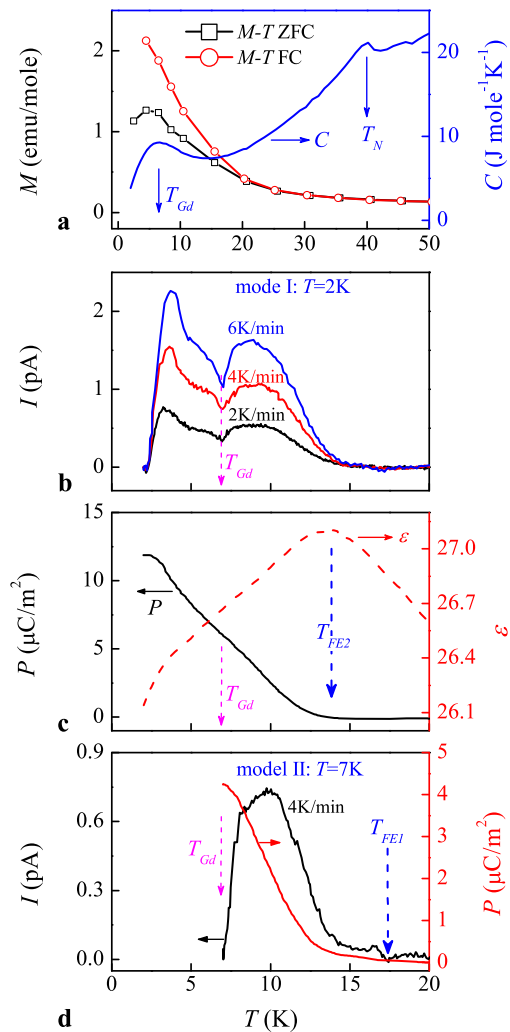


**Fig. 1** (a) Measured  $M(T)$  data under the ZFC and FC conditions with measuring field of 1000 Oe and measured  $C(T)$  data at zero field. (b) Measured pyroelectric current  $I(T)$  in mode I at three different warming rates (2, 4, 6 K/min) under  $H = 0$ . (c) Measured  $P(T)$  and  $\epsilon(T)$  data in mode I. (d) Measured  $I(T)$  and  $P(T)$  data in model II

spins. This disadvantage restricts a probe of the magnetic transitions from the Mn spin ordering. Roughly, it can be believed that the Gd<sup>3+</sup> spins evolve gradually from paramagnetic (PM) state into spin-glass-like state and eventually experience the AFM ordering at  $\sim 7$  K, which is obviously the Gd AFM ordering point  $T_{Gd}$  [34]. The Mn spin ordering sequence, however, can be partially observed from the  $C$ – $T$  data with a clear peak at  $T = T_N \sim 40$  K, which is interpreted as the onset of an incommensurate AFM phase [17, 20, 34]. A broad specific heat peak at  $T_{Gd} \sim 7$  K is also identified. Unfortunately, no clear anomaly of the  $C$ – $T$  curve between  $T = 7$  K to 40 K is observed, and earlier data on single crystal GMO didn't reveal such anomaly either [34, 35]. However, this does not exclude the possible Mn spin ordering in this  $T$ -range. In fact, the CS ordering may not generate clear feature in the  $C$ – $T$  curve for polycrystalline

samples, as shown for the case of DyMnO<sub>3</sub> and TbMnO<sub>3</sub> [25, 35].

We then turn to the ferroelectricity. We also take two different modes of the measurement in order to distinguish the effect of the Gd spin order at low  $T$  on the ferroelectricity. In mode I, the samples were cooled down to  $T = 2 \text{ K} < T_{\text{Gd}}$  under the poling field, while they were cooled down to  $T \sim T_{\text{Gd}} = 7 \text{ K}$  under the same poling field in mode II. Then the pyroelectric current  $I(T)$  was measured in the warming sequence. The measured  $I(T)$  data in mode I at three different warming rates (2, 4, 6 K/min) under  $H = 0$ , shown in Fig. 1(b), clearly exhibits two broad peaks below  $T \sim 14 \text{ K}$ . These peaks together with the dip do not show any shift along the  $T$ -axis for the three warming rates, indicating no contribution other than the polarization current in the measured  $I(T)$  data [36, 37]. Our data are consistent with earlier results on single crystal GMO [23], implying that the Mn CS order, developed by coupling with the Gd AFM order via the Mn<sup>3+</sup>–Gd<sup>3+</sup> spin interaction, disappears above  $T \sim 14 \text{ K}$ . We define this point as  $T_{\text{FE}2} = 14 \text{ K}$ , the Curie point for the ferroelectricity.

It should be mentioned that the two peaks sandwich a dip at  $T \sim T_{\text{Gd}}$ , indicating that the pyroelectric current is sensitive to the Gd spin ordering, which is hard to detect in the  $P(T)$  data to be shown below. Therefore, the pyroelectric current can be a good probe to the spin ordering sequence and relevant ME effect in GMO.

The evaluated  $P(T)$  curves from the three  $I(T)$  curves are almost overlapped, and one curve is plotted in Fig. 1(c), where the measured dielectric constant  $\varepsilon$  at 10 kHz as a function of  $T$  is also presented. The dielectric peak location at  $T_{\text{FE}2} \sim 14 \text{ K}$  is reasonable. The measured  $P$  increases gradually with decreasing  $T$  down to  $\sim 2 \text{ K}$ , with a weak bump at  $T \sim T_{\text{Gd}}$ . The above results allow us to claim that GMO is not simply A-AFM ordered. Instead, it must accommodate the Mn CS order or more, which are responsible for the polarization generation.

To proceed, we present in Fig. 1(d) the measured  $I(T)$  and  $P(T)$  data in mode II at 4 K/min warming rate, noting that no Gd spin order is available in this mode. It is seen that the measured  $P$  is much smaller than that obtained in model I, but the major difference here is that the measured  $P$  can sustain up to  $T = T_{\text{FE}1} \sim 17.5 \text{ K} > T_{\text{FE}2}$ . This substantial difference in the  $P(T)$  data for the two modes does unveil the role of the Gd spin ordering in modulating the ferroelectricity. The measured  $P$  in mode II is solely attributed to a specific Mn CS order (hereafter called the Mn CS phase I) in this case. In mode I, the measured  $P$  must be attributed to a Mn CS phase II other than the Mn CS phase I, and probably to the Gd spin order simultaneously. This Mn CS phase II is accompanied with the Gd spin order, also indicating the remarkable Mn<sup>3+</sup>–Gd<sup>3+</sup> spin interaction.

It is noted that the Mn CS phase I and phase II have their ordering points at  $T_{\text{FE}1}$  and  $T_{\text{FE}2}$ , respectively, indicating

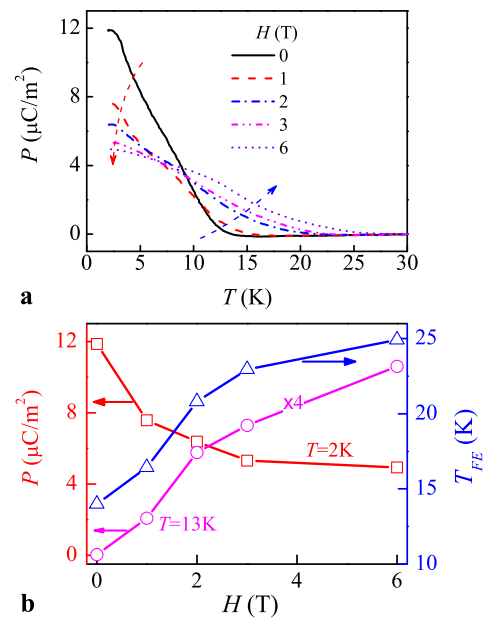


**Fig. 2** (a) Measured  $P$ – $T$  curves under various  $H$  and (b) evaluated  $P(H)$  dependences at  $T = 2 \text{ K}$  and  $T = 13 \text{ K}$ . The evaluated Curie point  $T_{\text{FE}}$  as a function of  $H$  is also plotted in (b)

that the phase I has higher stability than the phase II. The dip in the  $I(T)$  curves in mode I indicates that the Gd spin ordering can modulate the ferroelectricity, also. Therefore, as noted earlier, the origin for ferroelectricity in GMO is quite complicated.

Given the fact that the Gd spin order is sensitive to magnetic field  $H$ , one can further reveal the roles of these Mn CS phases and the Gd spin order by measuring the response of  $P$  to  $H$  over a broad  $T$ -range. The measured  $P(T)$  curves in mode I at various  $H$  are presented in Fig. 2(a), while Fig. 2(b) shows the measured  $P$  at  $T = 2 \text{ K}$  and  $T = 13 \text{ K}$ , and evaluated Curie point  $T_{\text{FE}}$  as a function of  $H$ . It is seen that the  $H$ -dependence of  $P$  is divided into two regimes. Below  $T \sim 9 \text{ K}$ , the  $P$  is gradually suppressed by increasing  $H$ . However, above  $T \sim 9 \text{ K}$ , increasing  $H$  not only enhances  $P$  but also shifts  $T_{\text{FE}}$  to high  $T$ -side. These responses are remarkable at  $H < 3.0T$  but become weak at  $H > 3.0T$ . It is interested to note that the remnant  $P(T)$  curves at  $H > 3.0T$  are roughly consistent with that obtained in mode II, implying that magnetic field drives the Mn CS phase II back to the Mn CS phase I, although the evaluated  $T_{\text{FE}}$  is slightly higher than  $T_{\text{FE}1}$ .

The above results allow us to propose a simple scenario for the spin ordering and polarization generation in GMO, and a schematic drawing of the  $T$ – $H$  multiferroic phase diagram is plotted in Figs. 3(a) and 3(b) for modes I and II, respectively, where the dashed and light gray lines are plotted for reference and they do not apply in the two respective cases. For  $H = 0$ , upon cooling from high- $T$  paramagnetic state, the Mn spins develop the AFM order at

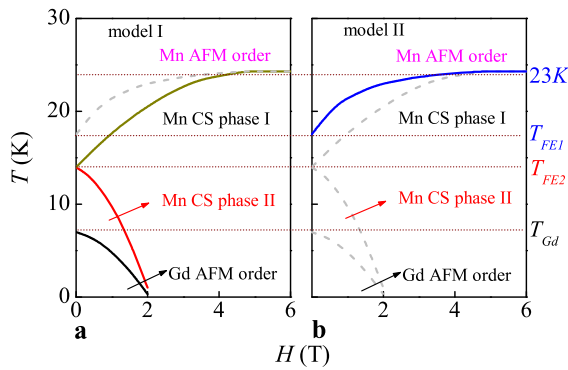


**Fig. 3** Proposed  $T$ – $H$  multiferroic phase diagrams for (a) model I and (b) model II. The solid lines represent the phase boundaries and the dashed and light gray lines are plotted for reference only

$T < T_N \sim 40$  K. In sequence, the Mn CS phase I is developed below  $T = T_{FE1} \sim 17.5$  K. Further cooling down to  $T_{Gd} \sim 7$  K and below, the Gd AFM order ensues, which also drives the Mn spin order from the Mn CS phase I into the Mn CS phase II via the Gd–Mn spin interaction. This phase II can sustain up to  $T_{FE2} \sim 14$  K upon the warming process. A field of  $H \sim 2.0$  T is sufficient to destroy the Gd AFM order [34], thus suppressing the Mn CS phase II and driving the reentrance of the Mn CS phase I. Both the Mn CS phases I and II contribute to the ferroelectricity. Here, an issue to be concerned is the  $H$ -driven expansion of the Mn CS phase I regime to higher  $T$ , while usually magnetic field prefers to break the Mn CS order in RMnO<sub>3</sub> [4, 5, 38]. Another issue is whether the Gd AFM spin order itself contributes to the ferroelectricity or not.

To this end, our measured data demonstrate that polycrystalline GMO offers not only significant ferroelectricity over a broad- $T$  range, but more importantly reveal the complicated spin-relevant origin for the ferroelectricity. Subsequently, we turn to the origin for the Mn CS orders in polycrystalline GMO while ideal GMO would prefer the A-AFM order at low  $T$ .

#### 4 Possible phase coexistence in GMO

Our primary motivation is that the inevitable disorder and defects in GMO, which is at the immediate edge of the A-AFM order and CS order may drive GMO from the A-AFM order into the coexistence of the two orders, in particularly in polycrystalline samples. In order to understand this issue, we investigate a simplified version of the semiquantum two-orbital double-exchange (TO-DE) model on manganites, in which the rare-earth spin is excluded for consideration. This allows us to catch the main stem of physics for the two-phase coexistence.

For simplicity, we start from a two-dimensional (2D)  $L \times L$  ( $12 \times 12$ ) square lattice on the  $x$ – $y$  plane under the periodic boundary conditions, which represents the Mn ionic

plane of RMnO<sub>3</sub> in orthorhombic structure. The Hamiltonian of the TO-DE model is written as [39, 40]:

$$H_{\text{TO-DE}} = - \sum_{(ij), \alpha\beta} t_{\alpha\beta}^r \Omega_{ij} c_{i\alpha}^+ c_{j\beta} + \sum_{(ij)} J_{ij}^{AF} S_i S_j + \sum_{[ij]} J_{ij}^{2b} S_i S_j + \lambda \sum_i (Q_{2i} \tau_{xi} + Q_{3i} \tau_{zi}) + \frac{1}{2} \sum_i (Q_{2i}^2 + Q_{3i}^2), \quad (1)$$

where the first term is the DE kinetic energy of  $e_g$  electrons,  $\alpha = |x^2 - y^2|$  and  $\beta = |3z^2 - r^2|$  are the two Mn- $e_g$  orbitals;  $c_{i\alpha\sigma}^+$  ( $c_{j\beta\sigma}$ ) is the creation (annihilation) operator for the  $e_g$  electron carrying spin  $\sigma$  on site  $i$ ;  $\Omega_{ij} = \cos(\theta_i/2) \cos(\theta_j/2) + \sin(\theta_i/2) \sin(\theta_j/2) \exp[-i(\Phi_i - \Phi_j)]$  with  $\theta_i$  and  $\Phi_i$  the angles of the  $t_{2g}$  spin  $S_i$  in the spherical coordinates. The actual hopping amplitudes  $t_{\alpha\beta}^r$  takes into account the different overlaps between the orbits along the  $x$ -axis and  $y$ -axis of the lattice:  $t_{\alpha\alpha}^x = t_{\alpha\alpha}^y = 3t_{\beta\beta}^x = 3t_{\beta\beta}^y = 3t_0/4$ ,  $t_{\alpha\beta}^y = t_{\beta\alpha}^y = -t_{\alpha\beta}^x = -t_{\beta\alpha}^x = \sqrt{3}t_0/4$ , and  $t_0$  ( $\sim 0.2$ – $0.5$  eV) is chosen as the energy unit. The second and third terms in Eq. (1) are the superexchange interactions between the NN and NNN  $t_{2g}$  spins along the  $b$ -axis. The fourth term in Eq. (1) is the electron-phonon coupling arising from the interaction between the  $e_g$  electron and MnO<sub>6</sub> octahedra distortion, and  $\lambda$  is the coupling constant with  $Q_{2i}$  and  $Q_{3i}$  scaling the  $(x^2 - y^2)$  and  $(3z^2 - r^2)$ -type Jahn–Teller distortions, respectively. We choose  $\lambda|Q_{2i}| = 1.5$  and  $Q_{3i} = -|Q_{2i}|/\sqrt{3}$  without losing the generality [39]. The orbital pseudospin operators are  $\tau_{xi} = \sum_{\sigma} (c_{i\alpha\sigma}^+ c_{i\beta\sigma} + c_{i\beta\sigma}^+ c_{i\alpha\sigma})$  and  $\tau_{zi} = \sum_{\sigma} (c_{i\alpha\sigma}^+ c_{i\alpha\sigma} - c_{i\beta\sigma}^+ c_{i\beta\sigma})$ . The last term of Eq. (1) is the elastic energy of the phonons. Typically, the temperature chosen for running the simulation is  $T = 0.002$  for the ground state, and details of the computation can be found in our earlier works [39].

In order to take into account the fluctuations from disorders and defects, we choose  $J_{2b} = 0.005$  but impose symmetrical perturbations to parameter,  $J_{ij}^{AF} = J_{ij}^{AF0} \pm \Delta J$ . The simulation is performed on a lattice whose ground state is the A-AFM at  $\Delta J = 0$  but close to the boundary between the A-AFM order and CS order, so that the effect of  $\Delta J$  on the spin structure. We choose  $J_{ij}^{AF0} = 0.07$ , which falls into the A-AFM region and close to the value of GMO [28–30, 41].

In order to identify the spin-ordered phase, we evaluate the spin configuration in real space and calculate the spin structure factor  $K(k) = \sum_{ij} (S_i S_j) \exp[ik(r_i - r_j)]/L^4$  in the momentum space. The polarization  $P$  is contributed from the asymmetric exchange striction mechanism, i.e. generated by the CS phase:

$$P \propto \frac{1}{L^2} \left\langle \sum_{(ij)} |e_{ij} \times (S_i \times S_j)| \right\rangle_T, \quad (2)$$

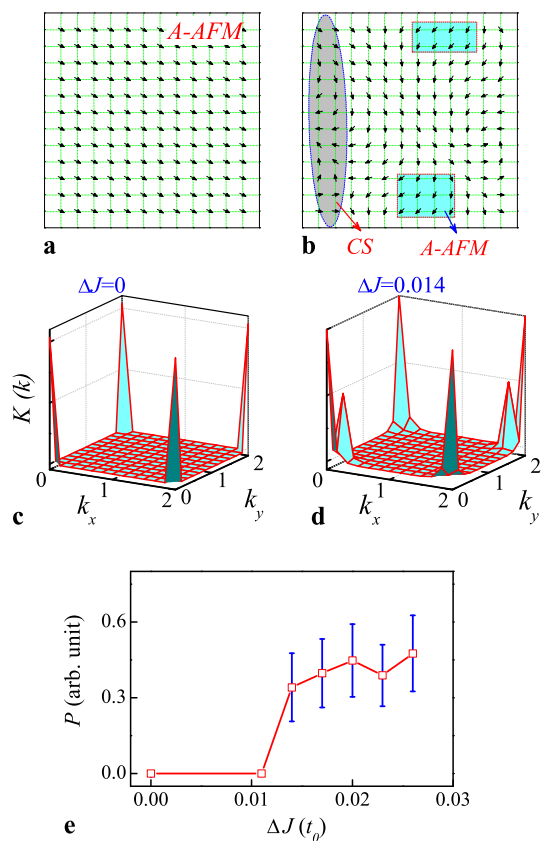


**Fig. 4** Snapshots of the Mn spin configuration for (a)  $\Delta J = 0$  with A-AFM phase and (b)  $\Delta J = 0.014$  with coexisting A-AFM phase and CS phase. The calculated  $K(\mathbf{k})$  spectra are plotted for (c)  $\Delta J = 0$  and (d)  $\Delta J = 0.014$ , respectively. (e) Evaluated  $P$  as a function of  $\Delta J$  at sufficiently low  $T$

where  $e_{ij}$  denotes the unit vector connecting sites  $i$  and  $j$  [13, 14],  $S_i$  denotes the Mn spin at site  $i$ , and the  $\langle \dots \rangle_T$  represents the thermal configuration averaging. The Monte Carlo (MC) procedure of the  $t_{2g}$  spins is employed for the present calculation. At each MC step, the fermionic sector of the Hamiltonian is exactly diagonalized [39, 42]. The initial 15,000 MC steps are discarded for equilibration and the subsequent 5000 MC steps are retained for the data collection. Finally, the data are submitted to the zero- $T$  optimization to confirm the ground state.

The simulation is presented in Fig. 4 as a summary. Figure 4(a) shows the snapshot of the spin configuration for  $\Delta J = 0$ . The ground state is indeed the A-AFM phase where all the in-plane spins align in the ferromagnetic order. To further confirm this result, the  $K(\mathbf{k})$  spectrum is evaluated and shown in Fig. 4(c). A peak of  $K(\mathbf{k})$  appears at  $\mathbf{k} = (0, 0)$ , indicating an in-plane FM order, is clearly displayed. Due to the periodic boundary condition, the identical peaks at  $\mathbf{k} = (0, 2)$ ,  $\mathbf{k} = (2, 0)$ , and  $\mathbf{k} = (2, 2)$  are observed, also.

When  $\Delta J > 0$  is applied, a clear transition of the spin order from the A-AFM state to the CS state is observed. One example is shown at  $\Delta J = 0.014$ , and the simulated results

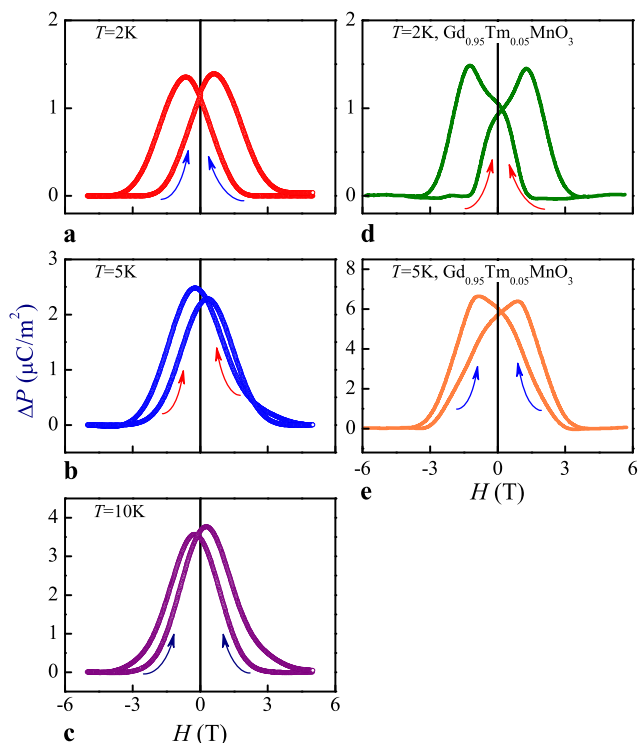


**Fig. 5** Measured  $\Delta P$ - $H$  hysteresis at (a)  $T = 2$  K, (b)  $T = 5$  K, and (c)  $T = 10$  K, for polycrystalline GMO.  $\Delta P = P(H) - P(5T)$ . The measured  $\Delta P$ - $H$  hysteresis for polycrystalline GTMO is shown in (d)  $T = 2$  K and (e)  $T = 5$  K

are plotted in Figs. 4(b) and 4(d). It is clearly shown that the lattice is mixed with the A-AFM phase and CS phase, as marked by the color regimes. The main peaks of  $K(\mathbf{k})$  appears at  $\mathbf{k} = (0, 0)$ , indicating the A-phase and the other two main peaks at  $\mathbf{k} = \pm\pi(1, 1)/12$  correspond to the CS phase with the spiral periodicity of 12 along the  $x$ -axis and  $y$ -axis, confirming the existence of the CS phase in addition to the A-AFM phase. The as-evaluated polarization  $P$  as a function of  $\Delta J$  is also presented in Fig. 4(e), suggesting that a nonzero  $P$  appears at  $\Delta J > 0.01$ . With increasing  $\Delta J$ , the ferroelectric domains associated with the CS domains gradually emerge, leading to enhanced  $P$ .

The present simulation thus demonstrates that even ideal GMO lattice itself prefers the A-AFM order, sufficiently weak fluctuations arising from the disorder/defects in the lattice may lead to appearance of the CS phase, thus contributing to the ferroelectricity, as observed in earlier and present experiments on polycrystalline GMO. This phase coexistence scenario, as a compliment to the above scenario on the ferroelectricity arising from the Mn spin order coupled with the Gd AFM order, represents a comprehensive understanding to the multiferroicity in polycrystalline GMO.

As complimentary evidence with the above simulated results, we measured the isothermal  $P$ - $H$  hysteresis loops at several low  $T$ , as shown in Figs. 5(a)-5(c), while the sam-

ples were cooled down to  $T = 2$  K before the measurement. The measurement was done by setting the  $P$  value at  $H = 5$  T as reference and then cycling  $H$  between (5 T,  $-5$  T), so that the variation of  $P$ ,  $\Delta P(H)$  was probed. It is shown that the  $\Delta P(H)$  data over one  $H$ -cycle do not overlap and significant  $P$ - $H$  hysteresis is recorded for each case. Unfortunately, neutron scattering evidence to conform the evolution of magnetic structure associated with the  $P$ - $H$  hysteresis is lacking. Nevertheless, such  $P$ - $H$  hysteresis loops suggest the nature of first-order phase transitions and a straightforward consequence is that polycrystalline GMO may accommodate the CS order in addition to the ground state A-AFM order. In fact, these loops show reasonable physics and can be understood from the point of view of multiferroic domain reversal. If the FE domains are interlocked with the Mn CS domains, these  $P$ - $H$  loops can be well explained. First, at low  $T$  (2 K), the butterfly loop is remarkable and more symmetrical, indicating a coercivity of  $\sim 0.7$  T. The loops at higher  $T$  become thinner and asymmetrical with lower coercivity. Second, the maximal  $\Delta P(H)$  increases with increasing  $T$ , indicating that the multiferroic domains reverse more easily at higher  $T$ , a reasonable phenomena.

Nevertheless, as mentioned in Sect. 1, in addition to the intrinsic structural and chemical disorder, the polycrystalline nature of the samples under measurements may also impose some extrinsic artifacts such as grain boundary pinning of the FE domain reversal, etc. These may be the source for the claimed phase coexistence and  $P$ - $H$  hysteresis. To clarify this issue, we also present in Figs. 5(d) and 5(e) the measured  $P$ - $H$  hysteresis loops for the polycrystalline GTMO sample at  $T = 2$  K and 5 K, respectively, noting the fact that the GTMO sample has the similar microstructures as the GMO sample. As expected, the polycrystalline GTMO sample also shows remarkable  $P$ - $H$  loops at the two temperatures. The coercivity of the GTMO at  $T = 2$  K and 5 K is  $\sim 1.3$  T and  $\sim 0.8$  T, respectively, slightly higher than  $\sim 0.7$  T and  $\sim 0.4$  T for the GMO sample. Since the GTMO is occupied with the  $ab$ -plane CS phase coexisting with minor A-AFM phase, the higher coercivity and larger polarization variation in polycrystalline GTMO than polycrystalline GMO are reasonable. The existence of the  $P$ - $H$  loops indicates the FE domain reversal in response to  $H$ -switching. This partially supports that the polycrystalline GMO sample does accommodate the CS phase.

The above results repeatedly suggest that the polycrystalline GMO does accommodate the Mn CS phase responsible for the ferroelectricity. In more words, the Mn CS phase is allowed to coexist with the A-AFM phase. Such a scenario allows us to understand the complicated multiferroic behaviors in polycrystalline GMO, although the microscopic origins for the existence of the Mn CS phase in addition to the A-AFM phase remain to be an issue in the experimental sense and no direct neutron data on the Mn CS phase

is available at this stage. It is believed that the microscopic electronic inhomogeneity would be one of the reasons for the appearance of the Mn CS phase.

## 5 Conclusion

As a summary, the present work reveals the ferroelectricity in polycrystalline GMO, while GMO in the ideal situation prefers the A-AFM order. The complicated multiferroic behaviors of polycrystalline GMO in response to temperature, magnetic field, and electrical poling mode have been revealed. The Gd spin ordering at low  $T$  has substantial modulating effect on the Mn CS phase. Based on our simulation on the two-orbit double exchange model with disorder/defects induced fluctuations of the spin interaction, plus the measured remarkable  $P$ - $H$  hysteresis, it is suggested that the polycrystalline GMO accommodates the CS ordered phase coupled with the A-AFM phase. The present work represents a comprehensive understanding to the ferroelectricity in polycrystalline GMO in terms of the Gd-Mn spin interaction consequence.

**Acknowledgement** This work was supported by the National 973 Projects of China (Grant No. 11234005), the Natural Science Foundation of China (Grants No. 11074113 and No. 50832002), and the Priority Academic Program Development of Jiangsu Higher Education Institutions, China.

## References

1. S.-W. Cheong, M. Mostovoy, Nat. Mater. **6**, 13 (2007)
2. K.F. Wang, J.-M. Liu, Z.F. Ren, Adv. Phys. **58**, 321 (2009)
3. S. Dong, J.-M. Liu, Mod. Phys. Lett. **26**, 1230004 (2012)
4. T. Goto, T. Kimura, G. Lawes, A.P. Ramirez, Y. Tokura, Phys. Rev. Lett. **92**, 257201 (2004)
5. T. Kimura, T. Goto, H. Shintani, K. Ishizaka, Y. Tokura, Nature **426**, 55 (2003)
6. Y. Yamasaki, S. Miyasaka, Y. Kaneko, J.-P. He, T. Arima, Y. Tokura, Phys. Rev. Lett. **96**, 207204 (2006)
7. W.D. Wu, Y. Horibe, N. Lee, S.-W. Cheong, J.R. Guest, Phys. Rev. Lett. **108**, 077203 (2012)
8. T. Lottermoser, T. Lonkai, U. Amann, D. Hohlwein, J. Ihlinger, M. Fiebig, Nature **430**, 541 (2004)
9. N. Hur, S. Park, P.A. Sharma, J.S. Ahn, S. Guha, S.-W. Cheong, Nature **429**, 392 (2004)
10. K. Taniguchi, N. Abe, T. Takenobu, Y. Iwasa, T. Arima, Phys. Rev. Lett. **97**, 097203 (2006)
11. G.Q. Zhang, S. Dong, Z.B. Yan, Y.Y. Guo, Q.F. Zhang, S. Yunoki, E. Dagotto, J.-M. Liu, Phys. Rev. B **84**, 174413 (2011)
12. R.D. Johnson, L.C. Chapon, D.D. Khalyavin, P. Manuel, P.G. Radaelli, C. Martin, Phys. Rev. Lett. **108**, 067201 (2012)
13. T. Moriya, Phys. Rev. **120**, 91 (1960)
14. M. Mostovoy, Phys. Rev. Lett. **96**, 067601 (2006)
15. I.A. Sergienko, C. Sen, E. Dagotto, Phys. Rev. Lett. **97**, 227204 (2006)
16. S. Picozzi, K. Yamauchi, B. Sanyal, I.A. Sergienko, E. Dagotto, Phys. Rev. Lett. **99**, 227201 (2007)

17. T. Kimura, S. Ishihara, H. Shintani, T. Arima, K.T. Takahashi, K. Ishizaka, Y. Tokura, *Phys. Rev. B* **68**, 060403(R) (2003)
18. S. Ishiwata, Y. Kaneko, Y. Tokunaga, Y. Taguchi, T. Arima, Y. Tokura, *Phys. Rev. B* **81**, 100411(R) (2010)
19. S. Landsgesell, A. Maljuk, T.C. Hansen, O. Prokhnenko, N. Aliouane, D.N. Argyriou, *Phys. Rev. B* **80**, 014412 (2009)
20. T. Kimura, G. Lawes, T. Goto, Y. Tokura, A.P. Ramirez, *Phys. Rev. B* **71**, 224425 (2005)
21. R. Feyerherm, E. Dudzik, A.U.B. Wolter, S. Valencia, O. Prokhnenko, A. Maljuk, S. Landsgesell, N. Aliouane, L. Bouchenoire, S. Brown, D.N. Argyriou, *Phys. Rev. B* **79**, 134426 (2009)
22. T. Goto, Y. Yamasaki, H. Watanabe, T. Kimura, Y. Tokura, *Phys. Rev. B* **72**, 220403(R) (2005)
23. K. Noda, S. Nakamura, J. Nagayama, H. Kuwahara, *J. Appl. Phys.* **97**, 10C103 (2005)
24. N. Zhang, Y.Y. Guo, L. Lin, S. Dong, Z.B. Yan, X.G. Li, J.-M. Liu, *Appl. Phys. Lett.* **99**, 102509 (2011)
25. N. Zhang, S. Dong, G.Q. Zhang, L. Lin, Y.Y. Guo, J.-M. Liu, *Appl. Phys. Lett.* **98**, 012510 (2011)
26. B. Lorenz, Y.Q. Wang, C.W. Chu, *Phys. Rev. B* **76**, 104405 (2007)
27. N. Lee, Y.J. Choi, M. Ramazanoglu, W. Ratcliff, V. Kiryukhin, S.-W. Cheong, *Phys. Rev. B* **84**, 020101(R) (2011)
28. M. Mochizuki, N. Furukawa, N. Nagaosa, *Phys. Rev. Lett.* **105**, 037205 (2010)
29. M. Mochizuki, N. Furukawa, N. Nagaosa, *Phys. Rev. B* **84**, 144409 (2011)
30. M. Mochizuki, N. Furukawa, *Phys. Rev. B* **80**, 134416 (2009)
31. A. Malashevich, D. Vanderbilt, *Phys. Rev. Lett.* **101**, 037210 (2008)
32. T. Arima, T. Goto, Y. Yamasaki, S. Miyasaka, K. Ishii, M. Tsubota, T. Inami, Y. Murakami, Y. Tokura, *Phys. Rev. B* **72**, 100102(R) (2005)
33. L. Li, L. Lin, Z.B. Yan, Q.Y. He, J.-M. Liu, *J. Appl. Phys.* **112**, 034115 (2012)
34. J. Hemberger, S. Lobina, H.-A. Krug von Nidda, N. Tristan, V.Y. Ivanov, A.A. Mukhim, A.M. Balbashov, A. Loidl, *Phys. Rev. B* **70**, 024414 (2004)
35. N.P. Kumar, G. Lalitha, P.V. Reddy, *Phys. Scr.* **83**, 045701 (2011)
36. Y.Y. Guo, H.M. Liu, D.P. Yu, J.-M. Liu, *Phys. Rev. B* **85**, 104108 (2012)
37. X.W. Dong, S. Dong, K.F. Wang, J.G. Wan, J.-M. Liu, *Appl. Phys. Lett.* **96**, 242904 (2010)
38. N. Aliouane, D.N. Argyriou, J. Stempfer, I. Zegkinoglou, S. Landsgesell, M.v. Zimmermann, *Phys. Rev. B* **73**, 020102(R) (2006)
39. S. Dong, R. Yu, S. Yunoki, J.-M. Liu, E. Dagotto, *Phys. Rev. B* **78**, 155121 (2008)
40. T. Hotta, A. Feiguin, E. Dagotto, *Phys. Rev. Lett.* **86**, 4922 (2001)
41. Y. Yamasaki, H. Sagayama, N. Abe, T. Arima, K. Sasai, M. Matsuura, K. Hirota, D. Okuyama, Y. Noda, Y. Tokura, *Phys. Rev. Lett.* **101**, 097204 (2008)
42. C.L. Lu, S. Dong, K.F. Wang, J.-M. Liu, *Appl. Phys. A* **99**, 323 (2010)